applied sciences

Article

Probabilistic Seismic Sensitivity Analyses of High-Speed Railway Extradosed Cable-Stayed Bridges

Mingzhi Xie [1,2,*], Jinglian Yuan [1,2], Hongyu Jia [1,2], Yongqing Yang [1,2], Shengqian Huang [1,2] and Baolin Sun [3]

[1] School of Civil Engineering, Southwest Jiaotong University, Chengdu 610031, China; yuanjl1999@163.com (J.Y.); hongyu1016@swjtu.edu.cn (H.J.); yangyongqingx@163.com (Y.Y.); huangshengqian@swjtu.edu.cn (S.H.)
[2] National Key Laboratory of Bridge Intelligent and Green Construction, Southwest Jiaotong University, Chengdu 611756, China
[3] Department of Engineering Mechanics, Shijiazhuang Tiedao University, Shijiazhuang 050043, China; sunbaolinx@163.com
* Correspondence: mzxie@swjtu.edu.cn

Featured Application: This study is aimed at sensitivity of seismic fragility demand parameters caused by structural uncertainty of high-speed railway extradosed cable-stayed bridge considering the Yuanjiang extra-large bridge on Huaihua–Shangyang–Hengyang Railway in China. Based on the probability distribution and correlation of random parameters, a sampling analysis method is proposed herein. Furthermore, a dynamic 3D finite element model of the employed bridge is established by using OpenSEES nonlinear software with full consideration of the randomness of structural parameters using sampling analysis. Based on these findings, some important conclusions were drawn. We believe that our study makes a significant contribution to the literature because although existing studies have focused on static parameter sensitivity analyses and have provided evidence for the design and construction control of cable-stayed bridges, the dynamic sensitivity studies especially for the structural parameter uncertainty of high-speed railway extradosed cable-stayed bridges have not been extensively studied. Further, we believe that this paper will be of interest to the readership of your journal because our analysis employs innovative research techniques, and our findings have the potential to provide guidance for the seismic fragility analysis of high-speed railway extradosed cable-stayed bridges. This manuscript has not been published or presented elsewhere in part or in entirety and is not under consideration by another journal. We have read and understood your journal's policies, and we believe that neither the manuscript nor the study violates any of these. There are no conflicts of interest to declare.

Abstract: It is known that the extradosed cable-stayed bridge, a hybrid bridge, possesses the virtues of both classic cable-stayed bridges and girder bridges in mechanical behaviors. In this paper, the sensitivity of seismic fragility demand parameters (SFDP) of a high-speed railway extradosed cable-stayed bridge is studied systematically along with the consideration of structural parameter uncertainty. Based on the probability distribution and correlation of random parameters, the Latin hypercube sampling method is adopted herein. The dynamic 3D finite element model of the employed bridge is established by using powerful and attractive OpenSEES nonlinear software. A nonlinear incremental dynamic analysis is performed to consider the randomness of structural parameters using sampling analysis. Some important conclusions are drawn indicating that the structural design parameter uncertainty predominantly has influence on the SFDP for fragility analysis of bridge structures. The design parameters of extradosed cable-stayed bridges are categorized and identified as primary, secondary and insensitive parameters. The high sensitivity parameters of extradosed cable-stayed bridges for fragility analysis include friction coefficient of bearing, concrete bulk density, damping ratio, peak compressive strength of confined concrete, component size and peak strain of confined concrete. Additionally, the strength and strain of unconfined concrete cannot be ignored. Furthermore, the uncertainty of structural design parameters fails to be responsible for the cable force

check for updates

Citation: Xie, M.; Yuan, J.; Jia, H.; Yang, Y.; Huang, S.; Sun, B. Probabilistic Seismic Sensitivity Analyses of High-Speed Railway Extradosed Cable-Stayed Bridges. *Appl. Sci.* **2023**, *13*, 7036. https://doi.org/10.3390/app13127036

Academic Editor: José António Correia

Received: 23 May 2023
Revised: 7 June 2023
Accepted: 7 June 2023
Published: 11 June 2023

responses due to larger girder stiffness. The structural design parameter uncertainty has a significant influence on the responses of extradosed cable-stayed bridges for seismic fragility analysis.

Keywords: extradosed cable-stayed bridge; high-speed railway bridge; structural uncertainty; sensitivity analysis; SFDP

1. Introduction

Commonly extradosed cable-stayed bridges have the advantages of both ordinary cable-stayed bridges and of continuous girder bridges in their mechanical behaviors [1]. Because of their greater girder stiffness and smaller main girder height compared to ordinary cable-stayed bridges and similar continuous girder bridges, respectively, the extradosed cable-stayed is widely used. In addition, it is also the best choice when ordinary cable-stayed bridges and girder bridges are limited in the structural design or construction stages by the requirements of clearance, navigation, stiffness and aesthetics [2]. Usually, extradosed cable-stayed bridges with a main span length range from 150 m to 250 m have strong competitiveness in both mechanical performance and economy aspects as well as aesthetic appearance. Owing to the aforementioned characteristics of extradosed cable-stayed bridges, they have been used extensively for high-speed railway bridge engineering [3,4]. Compared with the ordinary cable-stayed bridge, the extradosed cable-stayed bridge shows great differences in the connection between the main girder and tower and in the relative stiffness of main girder to cable. Regardless of static or dynamic loads, the main girder of extradosed cable-stayed bridges is first taken as the primary enduring structure and then the remaining loads are arranged to the cable due to the stiffness difference [5,6].

In recent years, in the central and southwestern region of China, which is surrounded by the Pacific Rim and Eurasian seismic belts, an increasing number of extradosed cable-stayed bridges have been built as a result of the demanding development for both highway and railway transportation, and their seismic performances have attracted attention [7]. Compared with ordinary long-span cable-stayed bridges, the extradosed cable-stayed bridges usually adopt a fixed tower-girder system where the girders are either rigidly connected to piers to act as a continuous unit or are supported on bearings at each pier. Furthermore, the deck width of high-speed railway bridges is usually much smaller than that of highway cable-stayed bridges. Therefore, the longitudinal and transverse displacement control and internal force distribution of traditional long-span cable-stayed bridges and extradosed cable-stayed bridges under ground motion show great differences [8–12]. Meanwhile, as the extradosed cable-stayed bridge is a multi-stage statically indeterminate structure, the variation of structural parameters may affect responses or even result in damage due to subjection to ground motion [13]. The damage of large-span complex bridges under earthquakes not only affects their bearing safety, but also affects the transportation system; this will have a serious impact on train speed, evacuation and rescue after the earthquake as well as on the post-earthquake resilient structure [14–16]. Therefore, it is very important to study the parameter sensitivity of the seismic response of high-speed railway extradosed cable-stayed bridges, and to find the primary, secondary and insensitive parameters affecting the SFDP of the bridge. In addition, it is of great importance to explore the mechanical behavior and seismic design of such bridges under earthquakes [17].

Structural uncertainty is one of the main sources of uncertainty in the analysis of probabilistic seismic fragility in bridge engineering and has a great impact on bridge SFDP [18]. For bridge seismic fragility, the influence of structural random parameters mainly involving material parameters, structural characteristic parameters and dimension and load parameters cannot be ignored. Research has revealed that the variation of structural parameters is affected by many factors in the entire process of cable-stayed bridge construction, such as design, manufacturing, construction, environment, etc. [19], and that the uncertainty is mainly reflected in the parameter distribution and variation coefficient, which may cause deviations in finite element analysis. Therefore, it is necessary to further study the seismic response of high-speed railway extradosed cable-stayed bridges with the consideration of structural uncertainty. To explore the sensitivity of SFDP to uncertainty, it is of great significance to understand the bridge seismic functional damage. Finally, it also provides the basis for a resilience study of the post-earthquake bridge [20].

As is known, parameter sensitivity analysis is widely used in engineering field and outstanding achievements have been obtained in structural reliability analysis [21], finite element model modification [22] and parameter selection [23]. It is used to study the sensitivity of system output when model parameters, model input or initial conditions have changed. It provides a scientific basis for finding the main, secondary and insensitive parameters of structures [24], which is very important for reaching a comprehensive understanding of the mechanical behavior of high-speed railway extradosed cable-stayed bridges. Shi and Ran [25,26] took an extradosed cable-stayed bridge with a main span of 175 m as a subject in which to study the influence of concrete strength, theoretical thickness of components and concrete creep coefficient on the creep effect of the bridge by comparing different national codes. Then the influence on cable force, displacement and stress of the bridge were analyzed. Based on a railway extradosed cable-stayed bridge with main span length of 210 m, Feng et al. [7] studied the sensitivity of main girder displacement and force of pier bottom to the bearing and proposed methods for controlling girder deformation under transverse earthquakes. Xie et al. [27] studied the influence of random structural parameters on the stress and alignment of the main girder and deformation of pylon and cable forces by taking a hybrid girder cable-stayed bridge as a subject. In addition, compared with long-span cable-stayed bridges, the different mechanical behaviors of these two types of bridges were further explored [28]. Nariman [29] took a cable-stayed bridge as a case-study for a global sensitivity analysis based on the Monte Carlo sampling method, adopted to formulate the surrogate models and the sensitivity indices. With this method, it is useful to identify the rational effect and role of each parameter on the aerodynamic stability of structures. Wu et al. [30] studied the sensitivity of internal forces and the displacement of long-span cable-stayed bridge to the seismic model and structural parameters and found that the range of stochastic earthquake responses of the bridge structure was able to endanger the structural safety due to changes of the structural parameters. Jia et al. [31–33] studied the response of railway bridges under tri-directional spatial excitations, and presented a probability-based method for bridge risk assessment, providing some useful conclusions in the actual seismic design and analysis of railway bridges under tri-directional non-stationary multiple excitations. Mahdi et al. [34,35] studied seismic reliability, limit state risk evaluation and the probabilistic seismic assessment of railway bridges in Iran built many years in the past, through incremental dynamic analysis (IDA). Some useful suggestions were obtained, such as that the randomness of ground motions, uncertainty of structural design parameters and the soil–structure interaction should be completely considered in the seismic fragility analysis of bridge structures. However, to the best of the authors' knowledge, the parameters' uncertainties are rarely considered in the sensitivity analysis of extradosed cable-stayed bridges except for the static analysis. Obviously, there is especially still a lack of dynamic sensitivity studies concerning the probability characteristics such as random parameters distribution, the parameter correlation and variability for high-speed railway extradosed cable-stayed bridges.

Since there has been limited research on the seismic performance of extradosed cable-stayed railway bridges, this paper develops a probability reliability-based structural uncertainty analysis methodology for bridges under longitudinal and transverse ground motions selected from the Pacific Earthquake Engineering Research Center (PEER) of the United States, according to the location and site condition of the bridge. The structural uncertainty analysis is mainly aimed at the SFDP of high-speed railway extradosed cable-stayed bridges, and to explore their sensitivity to random parameters, so as to lay a foundation for the functional fragility of this type of bridge. Section 2 presents the fundamental theory of probability reliability by which random parameters can be sampled. Section 3 presents the nonlinear finite element model of the extradosed cable-stayed bridge based on the software OpenSEES (https://opensees.berkeley.edu/, accessed on 22 May 2023), fully considering the pile–soil interaction. In Section 4, the proposed probabilistic reliability for structural uncertainty analysis was implemented, and the sensitivity of bridge response influenced by random parameters was discussed. Finally, the SFDP for functional fragility of extradosed cable-stayed bridge can be determined. Conclusions and observations were drawn in Section 5. The schematic diagram of the probabilistic seismic sensitivity analyses is shown in Figure 1.

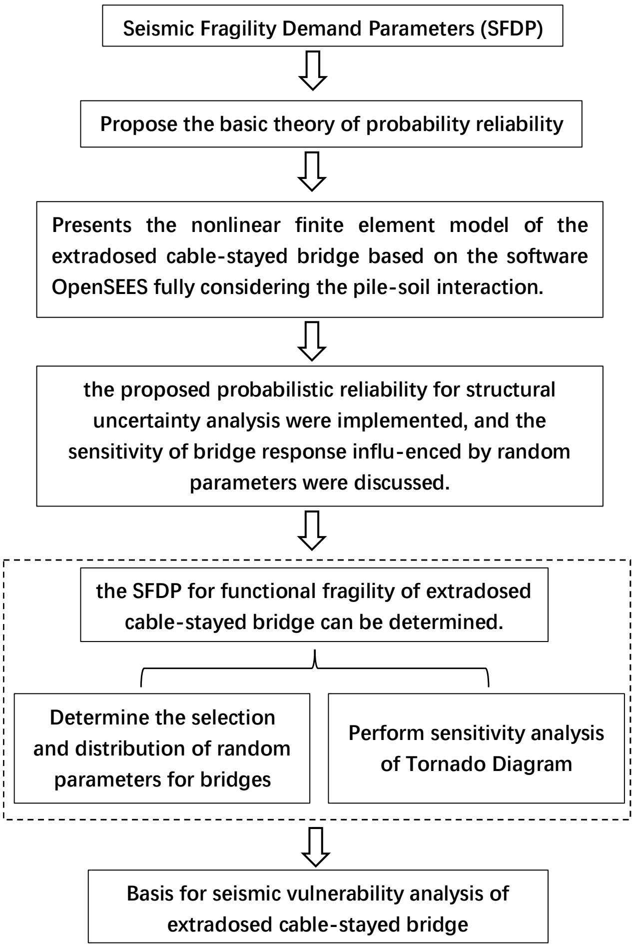

Figure 1. Schematic diagram of the probabilistic seismic sensitivity analyses.

2. Analysis of Structural Uncertainty Based on Probability Reliability

2.1. Latin Hypercube Sampling

Latin hypercube sampling [36,37] is a multi-dimensional stratified sampling method with high efficiency and stable estimation. It can obtain better results with fewer sampling times and is widely used in mathematical statistics and engineering practice fields. In view of the randomness of the structural parameters of the extradosed cable-stayed bridge, the method can be described as follows.

Suppose the random parameter of the bridge is X vector, which contains M random variables $X_1, X_2, X_3, \ldots \ldots, X_M$. Then assuming that the distribution function corresponding to each random variable X_i ($i = 1, 2, 3, \ldots \ldots, M$) is $\Phi_{x_i}(x)$, the M random variables are sampled N times to obtain an $N \times M$-dimensional matrix.

Divide $\Phi_{x_i}(x)$ into N non-lapped intervals $\varphi_{ij}(i = 1, 2, \cdots, M; j = 1, 2, \cdots, N)$, assuming that the probability of each interval is P_{ij}. It can be written as

$$P_{ij} = P(x_i \in \varphi_{ij}) \tag{1}$$

It is necessary to ensure that the cumulative probability of P_{ij} is 1, that is

$$\sum_{i=1}^{N} P_{ij} = 1 \tag{2}$$

In the case of equal probability, P_{ij} can be written as $1/N$. When sampling, $\varphi_{ij}(i = 1, 2, \cdots, M; j = 1, 2, \cdots, N)$ is selected according to its representative parameters. Generally, two methods can be adopted, namely the random selection and the center of gravity selection. For random selection, N random numbers Ran_j (j = 1, 2, 3, ... , N) are generated in the interval (0,1), then the random number $\mathrm{Ran_j}$ can be transformed into the random number R_j of the j-th interval by Equation (3).

$$R_j = \frac{Ran_j}{N} + \frac{j-1}{N} \ (\mathrm{j} = 1, 2, 3, \ldots\ldots, \mathrm{N}) \tag{3}$$

For R_j, it can be satisfied as

$$\frac{j-1}{N} < R_j < \frac{j}{N} \ (\mathrm{j} = 1, 2, 3, \ldots\ldots, \mathrm{N}) \tag{4}$$

Therefore, for the generated random number Ran_j (j = 1, 2, 3, ... , N), the value of the random variable in j intervals can be obtained according to Equation (5)

$$x_{ij} = \Phi_{x_i}{}^{-1}(R_j)(i = 1, 2, 3, \ldots\ldots, \mathrm{M};\ \ j = 1, 2, 3, \ldots\ldots, \mathrm{N}) \tag{5}$$

where $\Phi_{x_i}{}^{-1}$ is the inverse function of the distribution function Φ_{x_i} of the random variable x.

Similarly, for the selection of the interval center of gravity, x_{ij} can be written as

$$x_{ij} = \Phi_{x_i}{}^{-1}\left(\frac{Z_{ij} - 0.5}{N}\right)(i = 1, 2, 3, \ldots\ldots, \mathrm{M};\ \ j = 1, 2, 3, \ldots\ldots, \mathrm{N}) \tag{6}$$

where Z_{ij} is the interval rank of the j-th simulation of the i-th random variable.

The selection of the $\varphi_{ij}(i = 1, 2, \cdots, M;\ j = 1, 2, \cdots, N)$ interval in the sampling process is random. Each sampling of each random variable $\mathrm{X_i}$ (i = 1,2, 3, ... , M) corresponds of the randomness integer sequence (1, 2, 3, ... , N), and the corresponding sampling of M parameters can form a matrix Y with n rows and m columns. The matrix can be written as

$$Y = \begin{bmatrix} x_{11} & \cdots & x_{M1} \\ \vdots & \cdots & \vdots \\ x_{1N} & \cdots & x_{MN} \end{bmatrix} \tag{7}$$

Therefore, for the j-th sampling, the interval rank Z_{ij} of the random variable is the j-th row element of the matrix Y. Thus, the matrix Y is the sampling strategy of random variables. Despite the superiority of the Latin hypercube sampling approach, such as its high efficiency, stable estimation and better results with lower sampling times, it is insufficient to process the variance of the results. Therefore, according to the literature [38], the Latin hypercube sampling method is adopted herein. The random parameter $\mathrm{Ran_i}$ is generated by inverse transformation to generate random parameters that follow the distribution function, as shown in Equations (8) and (9).

$$x_i = \Phi^{-1}(Ran_i) \tag{8}$$

$$x_i' = \Phi^{-1}(1 - Ran_i) \tag{9}$$

Thus, the Latin hypercube sampling can be written as

$$\mathrm{y} = \frac{1}{2}\left[\Phi(x_i) + \Phi(x_i')\right] \tag{10}$$

2.2. Nataf Transformation of Model Parameter Correlation

Suppose a random vector $X = (X_1, X_2, X_3, \ldots \ldots, X_N)^{\mathrm{T}}$ is a non-normal distribution, and its joint cumulative distribution function is $F_x\,(x)$. Let $Y = (Y_1, Y_2, Y_3, \ldots \ldots, Y_N)^{\mathrm{T}}$ is a set of independent standard normal vectors. According to the equal probability edge change, the Equation (11) can be obtained as

$$\begin{cases} \Phi(Y_1) = F_{X_1}(x_1) \\ \Phi(Y_2) = F_{X_2|X_1}(x_2|x_1) \\ \vdots \\ \Phi(Y_n) = F_{X_n|X_1X_2,\cdots,Xn-1}(x_n|x_1, x_2, \cdots, x_{n-1}) \end{cases} \tag{11}$$

By inversing Equation (11), it can be written as

$$\begin{cases} Y_1 = \Phi^{-1}\left[F_{X_1}(x_1)\right] \\ Y_2 = \Phi^{-1}\left[F_{X_2|X_1}(x_2|x_1)\right] \\ \vdots \\ Y_n = \Phi^{-1}\left[F_{X_n|X_1X_2,\cdots,Xn-1}(x_n|x_1, x_2, \cdots, x_{n-1})\right] \end{cases} \tag{12}$$

Equation (12) is the Rosenblatt transformation, which can convert a group of non-normal random variables into equivalent independent normal random variables, and its conditional cumulative distribution function can be obtained by $F_x(x)$, that is

$$\begin{gathered} F_{X_n|X_1X_2,\cdots,Xn-1}(x_n|x_1, x_2, \cdots, x_{n-1}) = \\ \frac{1}{f_{X_1X_2\cdots Xn-1}(x_1, x_2, \cdots, x_{n-1})} \cdot \int_{-\infty}^{x_i} f_{X_1X_2\cdots Xn}(x_1, x_2, \cdots, x_n)dx_i \end{gathered} \tag{13}$$

When performing the Rosenblatt transformation, it is necessary to know the joint cumulative distribution function $F_x(x)$ of X. Assuming that the X correlation coefficient matrix is $\rho_X = \left[\rho_{x_ix_j}\right]_{n\times n}$ and its marginal probability density function is $f_{X_i}(x_i)$. While the marginal cumulative distribution function is a continuous increasing function, after mapping transformation, it is can be written as

$$Y_i = \Phi^{-1}\left[F_{X_i}(X_i)\right] \tag{14}$$

Then the correlation standard normal random vector Y can be obtained, and its correlation coefficient matrix is $\rho_Y = \left[\rho_{y_iy_j}\right]_{n\times n}$. Therefore, the joint probability density function of X can be written as

$$\begin{cases} f_X(x) = \det J_{YX}\varphi_n(y, \rho_Y) \\ \det J_{YX} = \prod\limits_{i=1}^{n} \frac{f_{X_i}(x_i)}{\varphi(y_i)} \end{cases} \tag{15}$$

Equation (15) is the Nataf distribution [39], and the correction coefficient of X can be written as

$$\rho_{X_iX_j} = \int_{-\infty}^{+\infty}\int_{-\infty}^{+\infty} \frac{x_i - \mu_{X_i}}{\sigma_{X_i}} \frac{x_j - \mu_{X_j}}{\sigma_{X_j}} \varphi_2\left(y_i, y_j, \rho_{Y_iY_j}\right)dy_idy_j \tag{16}$$

After determining the correlation coefficient matrix ρ_Y, the correlation normal vector Y can be transformed into an independent standard normal vector though orthogonal transformation. The mapping transformation can transform a non-normally distributed random vector X into a standard normal vector Y, and the correlation coefficient matrix of the Y vector can be calculated using Equation (16). The binary mapping transformation caused by the above-mentioned conversion is referred to as the Nataf transformation. Aiming at structural uncertainty, this paper introduces the Nataf transformation to consider the impact of concrete correlation, and then conducts sample calculation.

3. Numerical Analysis

3.1. Background of the Bridge

To study the influence of structural uncertainty on the SFDP of an extradosed cable-stayed bridge, the Yuanjiang extra-large bridge, a prestressed concrete extradosed cable-stayed bridge on the Huaihua–Shangyang–Hengyang Railway in China, with a span layout of 90 m + 180 m + 90 m, is taken as a case study. A photo of the bridge and a map with the location of the bridge are shown in Figure 2. It is a double-line railway bridge with a single-box single-cell girder. The width of the bridge deck and beam bottom are 13.6 m and 9.4 m, respectively. The varying heights of the girders are from 5 to 9.4 m. The height of the main girder changes in terms of a quadratic parabolic function. The materials of the main girder and pylons of the bridge are C55 concrete, and the cables are steel strand with a tensile strength of 1860 MPa. The piers are made of C35 reinforced concrete, with numbers ranging from 10# to 13#, and their heights are 22.9 m, 20.35 m, 21.85 m and 11.35 m, respectively, all of which are round-end cross sections. Additionally, the piles are also made of C35 reinforced concrete. Overall layout and detailed information are shown in Figure 3. The cross-section size and reinforcement of pylons and piers are shown in Figure 4. For the pylon reinforcement, all the steel bars are HRB400 with a diameter of 16mm except for vertical bars with a diameter of 25 mm. The yielding strength of HRB400 is 400 MPa. For the pier reinforcement, the vertical steel bars are HRB400 with a diameter of 16 mm, while the other steel bars are HPB300 bars, the yielding strength of which is 300 MPa with a diameter of 100 mm. In addition, the numbers illustrated in the pier reinforcement in Figure 4 show the information of 13# pier, while letters in brackets are for 10# to 12# pier as well as the information in table below the cross section. The support arrangement is shown in Figure 5.

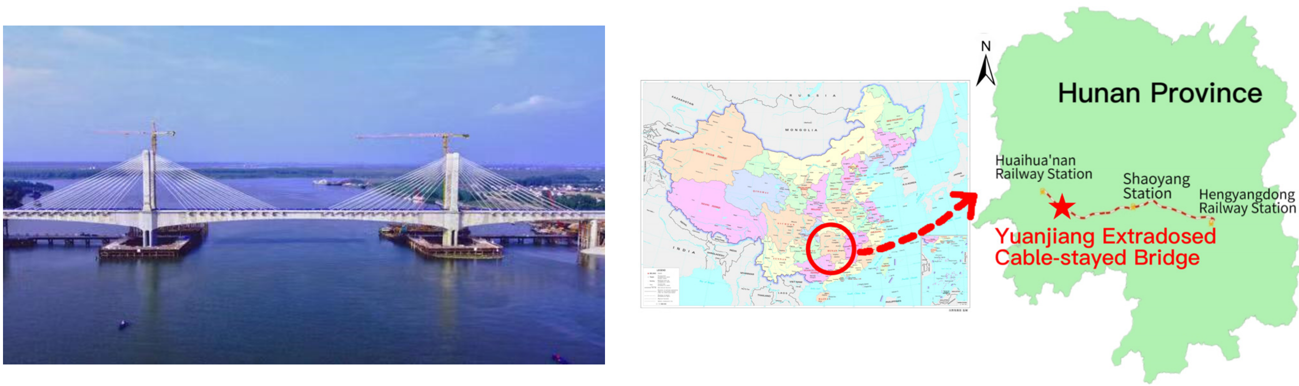

(**a**) (**b**)

Figure 2. Yuanjiang extradosed cable-stayed bridge and its location. (**a**) Yuanjiang extradosed cable-stayed bridge and (**b**) The location of the bridge in China.

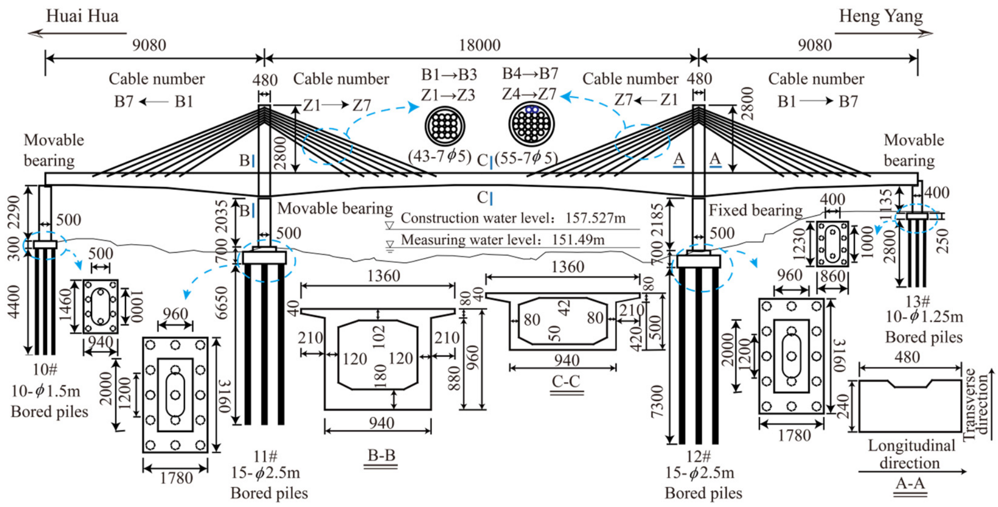

Figure 3. Layout of the extradosed cable-stayed bridge (units: cm).

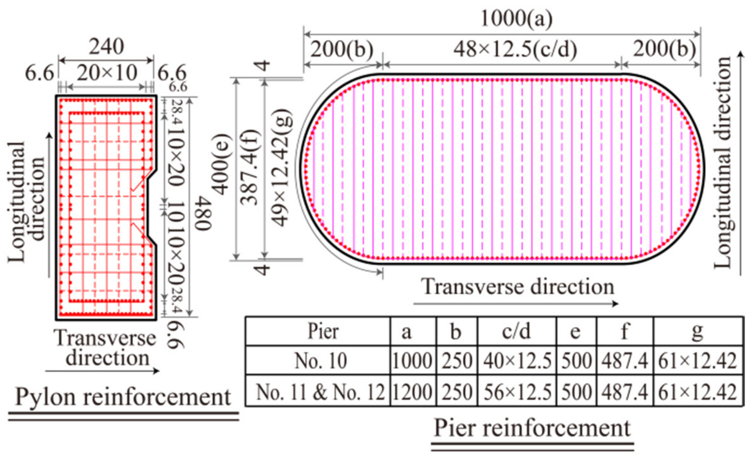

Figure 4. Cross-section size and reinforcement (units: cm).

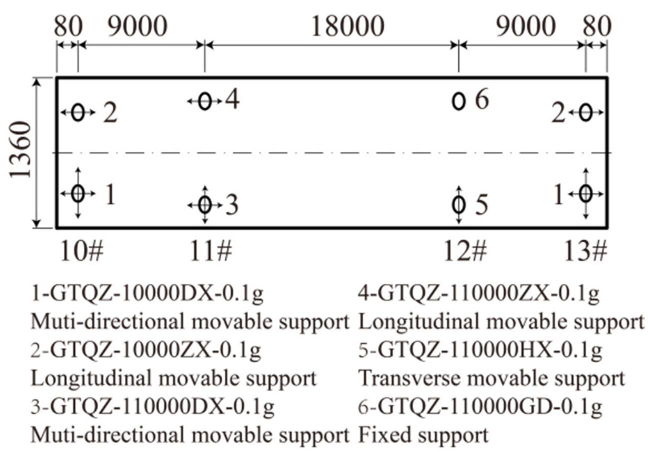

Figure 5. Support arrangement (units: cm).

3.2. Nonlinear Finite Element Model

A nonlinear dynamic numerical model of the extradosed cable-stayed bridge is built based on the nonlinear FEM software OpenSEES. As piers and pylons are vulnerable components under earthquakes, the main girder remains elastic. Therefore, the nonlinear beam-column element and fiber sections are used to model pylons, piers and piles, while the disp-beam-column element and elastic section are used to model the main girder. Due to the consolidation of the pylon and main girder, they are connected by rigid arms. The supports are modeled using a ZeroLength element which contains two nodes; the upper node is connected to the main girder by a rigid arm, and the bottom node is connected to the pier also by a rigid arm. The “m” method is adopted to consider the pile–soil effect, and the soil spring is also modeled using a ZeroLength element. In this bridge, the rigid arms connecting the bridge members are simulated using an elastic beam-column element. In the finite element model, the materials of the cables and main girder are Steel02 material and elastic material, respectively, while both rigid arms and soil springs use elastic material. Meanwhile, the material of the supports is elastic-perfectly plastic material. For pylons, piers and piles, the fiber sections consist of Concrete02 material and Steel02 material utilized to simulate their nonlinearity. The hysteresis model and constitutive relation of these two materials provided by the software OpenSEES are shown in Figures 6 and 7. Information about materials, simulation of components and the rigid arms is shown in Table 1, and the model parameters are summarized in Table 2. Finally, the detail of the dynamic 3D nonlinear dynamic finite element model of the employed bridge is shown in Figure 8.

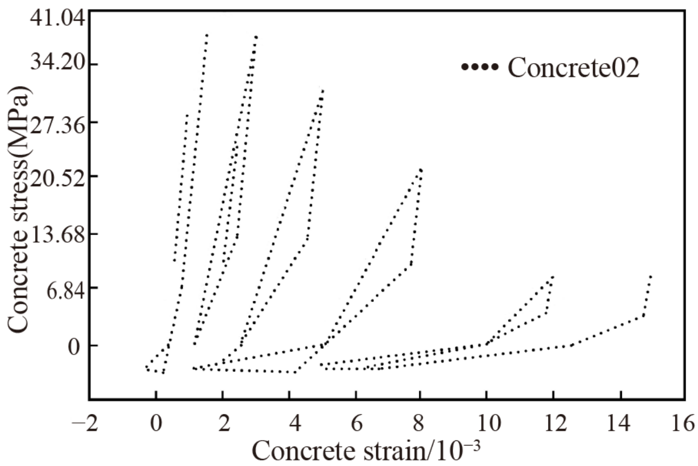

Figure 6. Hysteresis model of Concrete02 material.

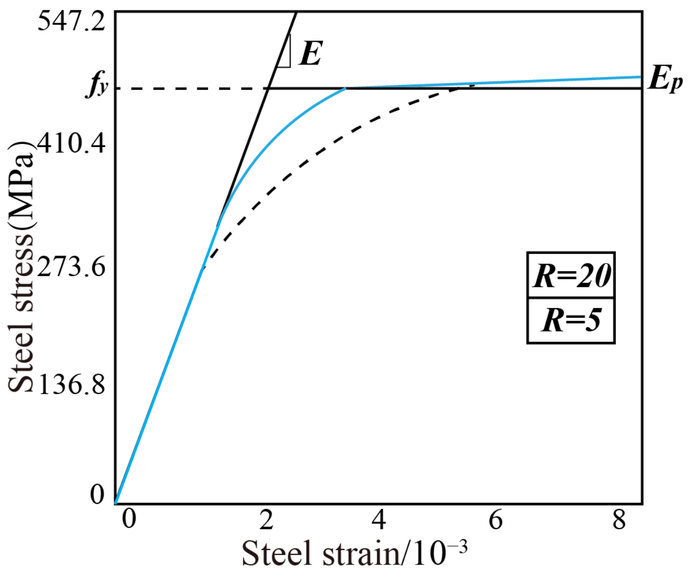

Figure 7. Constitutive relation of Steel02 material.

Table 1. Information regarding components, materials and the connecting rigid arm of extradosed cable-stayed bridge.

Component	Element Type	Material
Cable	Truss Element	Steel02 Material
Pylon	Nonlinear Beam-Column Element	Concrete02 Material Steel02 Material
Main girder	Elastic Beam-Column Element	Elastic Material
Bearing	ZeroLength Element	Elastic-Perfectly Plastic Material
Pier	Nonlinear Beam-Column Element	Concrete02 Material Steel02 Material
Pile	Nonlinear Beam-Column Element	Concrete02 Material Steel02 Material
Soil spring	ZeroLength Element	Elastic Material
Connecting rigid arm	Elastic Beam-Column Element	Elastic Material

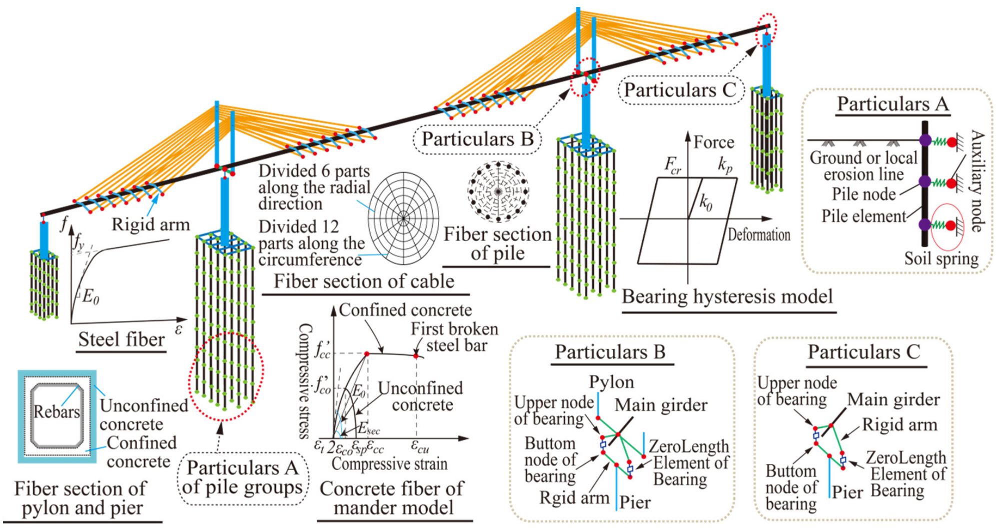

Figure 8. Finite element model of nonlinear dynamic analysis.

For the simulation of the pile–soil interaction, taking 13#pier as an example, the soil spring stiffness is calculated according to Equation (17) [40]

$$k = ab_1mz \tag{17}$$

where a is the equivalent soil thickness for calculating the soil spring stiffness, b_1 represents the calculated width of pile, m denotes the proportional coefficient of foundation coefficient, and z is the calculated depth of soil below the ground or local erosion line. Along the pile length, the soil layer is divided every 2 m, and the soil spring stiffness of longitudinal direction and transverse direction is added to the corresponding pile node. The soil spring model is shown in Figure 9, and detailed information regarding the pile–soil interaction is shown in Figure 10. Finally, the soil spring stiffness is shown in Table 3. According to the geological data of the soil layer, the foundation of the bridge passes through clay, sand pebbles and glutenite. The basic bearing capacity of the clay is 180 kPa, and the shear wave velocity range of the soil layer is 250≥ vs. >140, and the shear modulus is 114.76 MPa. The basic bearing capacity of sandy pebble soil is 350 kPa, the range of shear wave velocity is 500≥ vs. >250 and the shear modulus is 147.74 MPa. The basic bearing capacity of glutenite is 500 kpa, the shear wave velocity of soil layer vs. >500 and the shear modulus is 224 MPa.

Table 2. Summary of model parameters.

No.	Model Parameter	Pylon/Pier/Pile	Unit	No.	Model Parameter	Pylon/Pier/Pile	Unit
1	Peak compressive strength of confined concrete	48.1/30.55/30.55	MPa	7	Peak strain of unconfined concrete	0.002/0.002/0.002	
2	Ultimate compressive strength of confined concrete	9.62/6.11/6.11	MPa	8	Ultimate strain of unconfined concrete	0.004/0.004/0.004	
3	Peak strain of confined concrete	0.0045/0.0045/0.0045		9	Elastic modulus of concrete	36000/33000/33000	MPa
4	Ultimate strain of confined concrete	0.009/0.009/0.009		10	Yielding strength of steel	400/400/400	MPa
5	Peak compressive strength of unconfined concrete	37/23.5/23.5	MPa	11	Elastic modulus of steel	200000/200000/200000	MPa
6	Ultimate compressive strength of unconfined concrete	7.4/4.7/4.7	MPa	12	Thickness of cover layer	0.035/0.04/0.06	m
13	Elastic modulus of main girder	36,000	MPa	16	Friction coefficient of bearing	0.02	
14	Elastic modulus of cable	195,000	MPa	17	Damping ratio	0.05	
15	Yielding strength of cable	1860	MPa	18	Concrete bulk density	26.5	kN/m^3

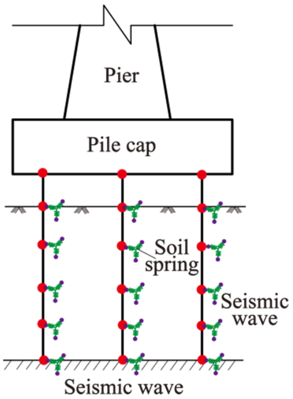

Figure 9. Soil spring model.

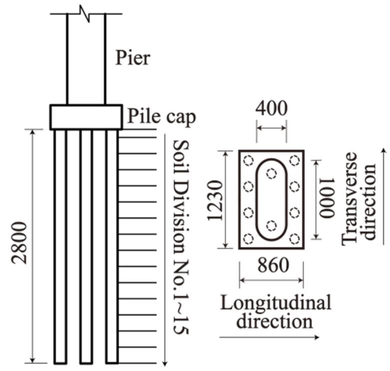

Figure 10. Detail of pile–soil (units: cm).

Table 3. Soil spring stiffness of 13# pier.

Calculation Parameters	**Longitudinal Direction Soil Spring Stiffness**					**Transverse Direction Soil Spring Stiffness**				
Soil Division	a (m)	b1 (m)	m (kN/m^4)	z (m)	k (kN/m)	a (m)	b1 (m)	m (kN/m^4)	z (m)	k (kN/m)
1.0	2.0	1.6	21,425.1	1.0	69,631.6	2.0	1.4	21,425.1	1.0	60,847.3
2.0	2.0	1.6	21,425.1	3.0	208,894.8	2.0	1.4	21,425.1	3.0	182,541.9
3.0	2.0	1.6	21,425.1	5.0	348,158.0	2.0	1.4	21,425.1	5.0	304,236.5
4.0	2.0	1.6	21,425.1	7.0	487,421.1	2.0	1.4	21,425.1	7.0	425,931.1
5.0	2.0	1.6	21,425.1	9.0	626,684.3	2.0	1.4	21,425.1	9.0	547,625.7
6.0	2.0	1.6	21,425.1	11.0	765,947.5	2.0	1.4	21,425.1	11.0	669,320.3
7.0	2.0	1.6	21,425.1	13.0	905,210.7	2.0	1.4	21,425.1	13.0	791,014.9
8.0	2.0	1.6	21,425.1	15.0	1,044,473.9	2.0	1.4	21,425.1	15.0	912,709.5
9.0	2.0	1.6	21,425.1	17.0	1,183,737.1	2.0	1.4	21,425.1	17.0	1,034,404.1
10.0	2.0	1.6	21,425.1	19.0	1,323,000.3	2.0	1.4	21,425.1	19.0	1,156,098.7
11.0	2.0	1.6	21,425.1	21.0	1,462,263.4	2.0	1.4	21,425.1	21.0	1,277,793.3
12.0	2.0	1.6	21,425.1	23.0	1,601,526.6	2.0	1.4	21,425.1	23.0	1,399,487.9
13.0	2.0	1.6	21,425.1	25.0	1,740,789.8	2.0	1.4	21,425.1	25.0	1,521,182.5
14.0	2.0	1.6	21,425.1	27.0	1,880,053.0	2.0	1.4	21,425.1	27.0	1,642,877.1
15.0	2.0	1.6	21,425.1	28.0	1,9496,84.6	2.0	1.4	21,425.1	28.0	1,703,724.4

3.3. Seismic Ground Motions

The bridge is located in a class II site according to the Code for Seismic Design of Railway Engineering in China. Therefore, the selection of target response spectra can be obtained according to the code that can be written as

$$S = \begin{cases} S_{\max}(5.5T + 0.45) & T < 0.1s \\ S_{\max} & 0.1s \le T \le T_g \\ S_{\max}\left(T_g/T\right) & T > T_g \end{cases} \tag{18}$$

where T_g is the site period that the characteristic period is 0.45, T represents the natural vibration period and $S_{\max}$ denotes the maximum value of horizontal design acceleration response spectra.

When the target response spectrum is determined, the ground motions can be selected by the principle of minimum mean square deviation. The mean square deviation can be derived as

$$\delta_{MSE} = \frac{\sum_i w(T_i)[\ln S_{at}(T_i) - \ln(fS_{ar}(T_i))]^2}{\sum_i w(T_i)} \quad (19)$$

where f is the linear scale factor for recording seismic response spectrum, $w(T_i)$ represents the weight coefficient, $S_{at}(T_i)$ is the target response spectrum and $S_{ar}(T_i)$ denotes the selected response spectrum.

This paper studies the influence of structural uncertainty on the SFDP of an extradosed cable-stayed bridge under longitudinal and transverse direction earthquakes. Owing to the aforementioned information of the location and site condition of the examined bridge, the natural ground motions are selected from PEER of the United States. The selected spectrums are shown in Figure 11.

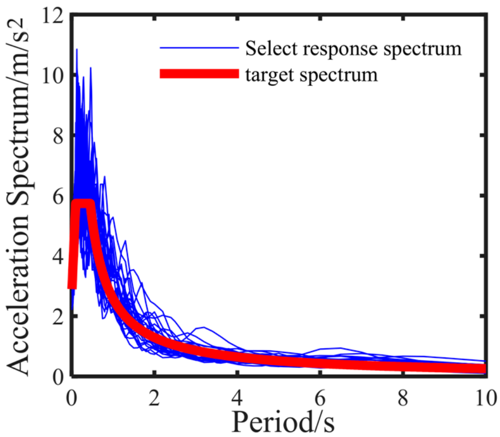

Figure 11. Target response spectrum and response spectrum.

4. Analysis of Structural Uncertainty

4.1. Random Parameter Selection and Distribution of the Bridge

In view of the parameter changes in the whole construction process of high-speed railway extradosed cable-stayed bridge, as well as the analysis of the static and dynamic characteristics of the bridge, the structural uncertainty research in this paper involves random parameters, such as material characteristic parameters, model constitutive parameters, dynamic characteristic parameters, structural size, etc. The parameters change according to the probability and statistics distribution, and the mean value is the design value as shown in Table 2. For example, for concrete bulk density, it satisfies the normal distribution, the standard deviation is 1.75 kN/m^3, and the mean value is 26.5 kN/m^3. For the damping ratio, it also satisfies the normal distribution, the coefficient of the variation is 0.2, and the standard deviation is 0.01. According to the literature [41,42], the parameters and their probability distribution are shown in Table 4.

Table 4. Probability distribution of uncertainty parameters.

No.	Uncertainty Parameter	Radom Variables	Variables Distribution Type	Standard Deviation	Coefficient of Variation	Unit
1	Peak compressive strength of confined concrete	$f_{c,core}$	Normal distribution	4.076/2.5889/2.5889	0.14	MPa
2	Ultimate compressive strength of confined concrete	$f_{cu,core}$	Normal distribution	0.8217/0.5218/0.5218	0.14	MPa
3	Peak strain of confined concrete	$e_{c,core}$	Normal distribution	0.0008/0.0008/0.0008	0.15	
4	Ultimate strain of confined concrete	$e_{cu,core}$	Normal distribution	0.002/0.002/0.0019	0.15	
5	Peak compressive strength of unconfined concrete	$f_{c,cover}$	Normal distribution	3.351/2.1283/2.1283	0.14	MPa
6	Ultimate compressive strength of unconfined concrete	$f_{cu,cover}$	Normal distribution	0.71/0.4509/0.4509	0.14	MPa
7	Peak strain of unconfined concrete	$e_{c,cover}$	Normal distribution	0.0003/0.0003/0.0003	0.15	
8	Ultimate strain of unconfined concrete	$e_{cu,cover}$	Normal distribution	0.0006/0.0006/0.0006	0.15	
9	Elastic modulus of concrete	E_c	Normal distribution	2880/2640/2640	0.08	MPa
10	Yielding strength of steel	f_y	Normal distribution	16/16/16	0.045	MPa
11	Elastic modulus of steel	E_y	Normal distribution	6600/6600/6600	0.10	MPa
12	Component size	D	Log-normal distribution	/	0.2	m
13	Thickness of cover layer	C	Normal distribution	0.0017/0.0019/0.0029	0.2	m
14	Elastic modulus of main girder	E_g	Normal distribution	2880	0.08	MPa
15	Elastic modulus of cable	E_{ca}	Normal distribution	19,500	0.1	MPa
16	Yielding strength of cable	f_{ca}	Normal distribution	74.4	0.04	MPa
17	Friction coefficient of bearing	m	Normal distribution	0.002	0.5	
18	Damping ratio	x	Normal distribution	0.005	0.2	
19	Concrete bulk density	g	Normal distribution	1.75	0.1	kN/m^3

When analyzing the nonlinear dynamic time history and fragility analysis of reinforced concrete bridges, the parameters' correlation of fiber section cannot be ignored and their influence should be considered in the analysis of structural uncertainty. The parameter correlation coefficient matrix of concrete is shown in Table 5.

Table 5. Correlation coefficient matrix of concrete material.

Correlation Coefficient	$f_{c,core}$	$f_{cu,core}$	$e_{c,core}$	$e_{cu,core}$	$f_{c,cover}$	$f_{cu,cover}$	$e_{c,cover}$	$e_{cu,cover}$
$f_{c,core}$	1	0.8			0.8	0.64		
$f_{cu,core}$	0.8	1			0.64	0.8		
$e_{c,core}$			1	0.8			0.8	0.64
$e_{cu,core}$			0.8	1			0.64	0.8
$f_{c,cover}$	0.8	0.64			1	0.8		
$f_{cu,cover}$	0.64	0.8			0.8	1		
$e_{c,cover}$			0.8	0.64			1	0.8
$e_{cu,cover}$			0.64	0.8			0.8	1

4.2. Sensitivity Analysis of Tornado Diagram

The sensitivity analysis of structural uncertainty to the SFDP of an extradosed cable-stayed bridge is an effective method to explore the laws of seismic response for high-speed railway bridges. Therefore, the "Tornado graphic method" is adopted for uncertainty analysis. This method is mainly used in the field of decision analysis in the early stage and is later introduced into the structural seismic damage assessment [43]. The basic idea behind this method for random parameter sensitivity analysis is to calculate the variation of SFDP relative to the input parameters, that is, to change a single parameter while other parameters remain unchanged, and to then conduct dynamic nonlinear time-history analysis to obtain a variation of the SFDP. The variation corresponding to each parameter is a horizontal bar graph, and n random variables correspond to n horizontal bar graphs. The wider the bar graph is, the more significant the influence of the random parameter is. Finally, the horizontal bar graphs are arranged from wide to narrow and from top to bottom. The basic idea of the method is shown in Figure 12.

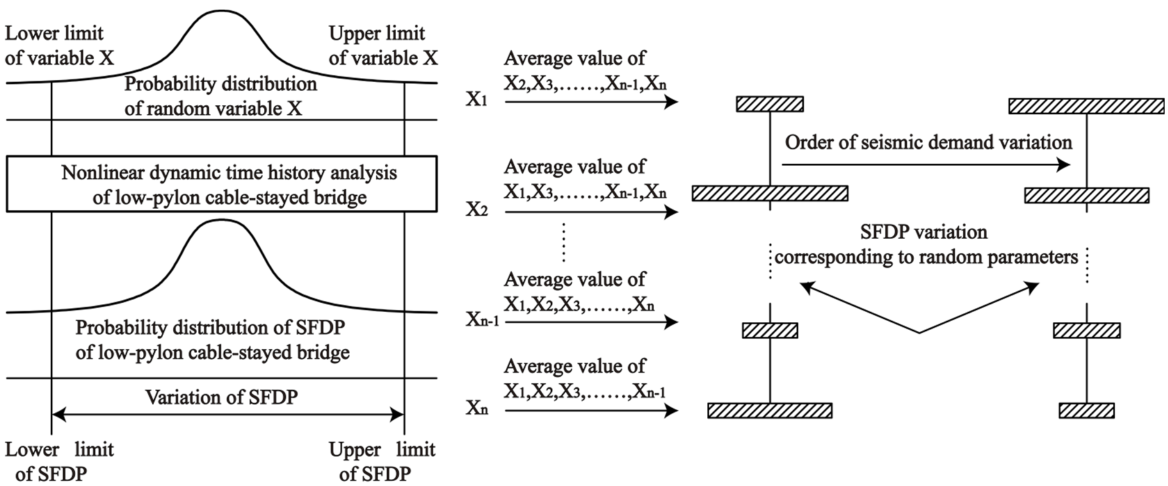

Figure 12. Principle of sensitivity analysis of the Tornado diagram.

The "Tornado graphic method" is used to analyze the sensitivity of structural uncertainty parameters. The specific steps can be described as follows:

(1) For high-speed railway bridge damage, the SFDP of an extradosed cable-stayed bridge are selected, such as angles of girder, support displacement, pier displacement, pier curvature, tower curvature and cable force;

(2) According to the probability distribution characteristics of each random parameter in Table 4 and considering the correlation, the upper limit and lower limit values can be determined using Latin hypercube sampling. Then, the single random variable x is changed, and its upper limit and lower limit values are brought into the dynamic analysis model, while the other parameters remain unchanged. Subsequently, the difference between the upper limit and lower limit value of the SFDP can be calculated. Finally, the difference is divided by the maximum value of the SFDP of a benchmark model, and its ratio is defined as the sensitivity of the SFDP;
(3) The sensitivity of the demand parameters to random variables can be analyzed after repeating step (2), and then the sensitivity as a "horizontal graph" of the random variable X can be drawn in the graph;
(4) Finally, a "horizontal graph" of each parameter can be obtained by repeating step (3); these can be arranged in descending order to analyze the parameter sensitivity of dynamic damage of the extradosed cable-stayed bridge.

4.3. Analysis of Structural Uncertainty

In this paper, the PGA of the selected ground motions are adjusted to 0.7 g for the desired requirements of elastic-plastic dynamic analysis and a nonlinear dynamic time-history analysis of extradosed cable-stayed bridges subjected to the longitudinal and transverse ground motions is carried out. The maximum responses in these models are defined as the reference value, and the results of each SFDP are shown in Table 6. According to the distribution of random parameters as shown in Table 4, the variation of each SFDP can be obtained by substituting the random parameters into OpenSEES model for calculation. According to the nonlinear results calculated by the selected ground motions, regression analysis of each seismic demand parameter is carried out to obtain the demand value so that the influence of the uncertainty of earthquake excitations can be considered. Subsequently, the sensitivity of each SFDP can also be obtained, which is divided by the reference value as in Table 6. Sensitivity results of the SFDP under the longitudinal ground motion are shown in Figure 13a–f.

Table 6. Result of SFDP under the benchmark model.

	Seismic Response in Longitudinal Direction				Seismic Response in Transverse Direction			
	10# Pier	**11# Pier**	**12# Pier**	**13# Pier**	**10# Pier**	**11# Pier**	**12# Pier**	**13# Pier**
Displacement of pier Top (units: m)	0.38	0.33	0.363	0.338	0.059	0.123	0.149	0.043
Main girder angle (units: $\times 10^{-3}$ rad)	2.40	3.10	2.90	1.70	1.90	3.40	3.10	2.20
Curvature of pier bottom($/\times 10^{-3}$)	3.80	4.70	3.30	7.60	0.12	1.10	1.30	0.11
Bearing displacement (units: m)	0.015	0.048	0.043	0.025	0.016	0.123	0.13	0.016
	11# Pylon		**12# Pylon**		**11# Pylon**		**12# Pylon**	
Curvature of pylon Bottom ($/\times 10^{-5}$)	4.10		−2.40		110		140	
Cable force (units: KN)	5905.6				6055.2			

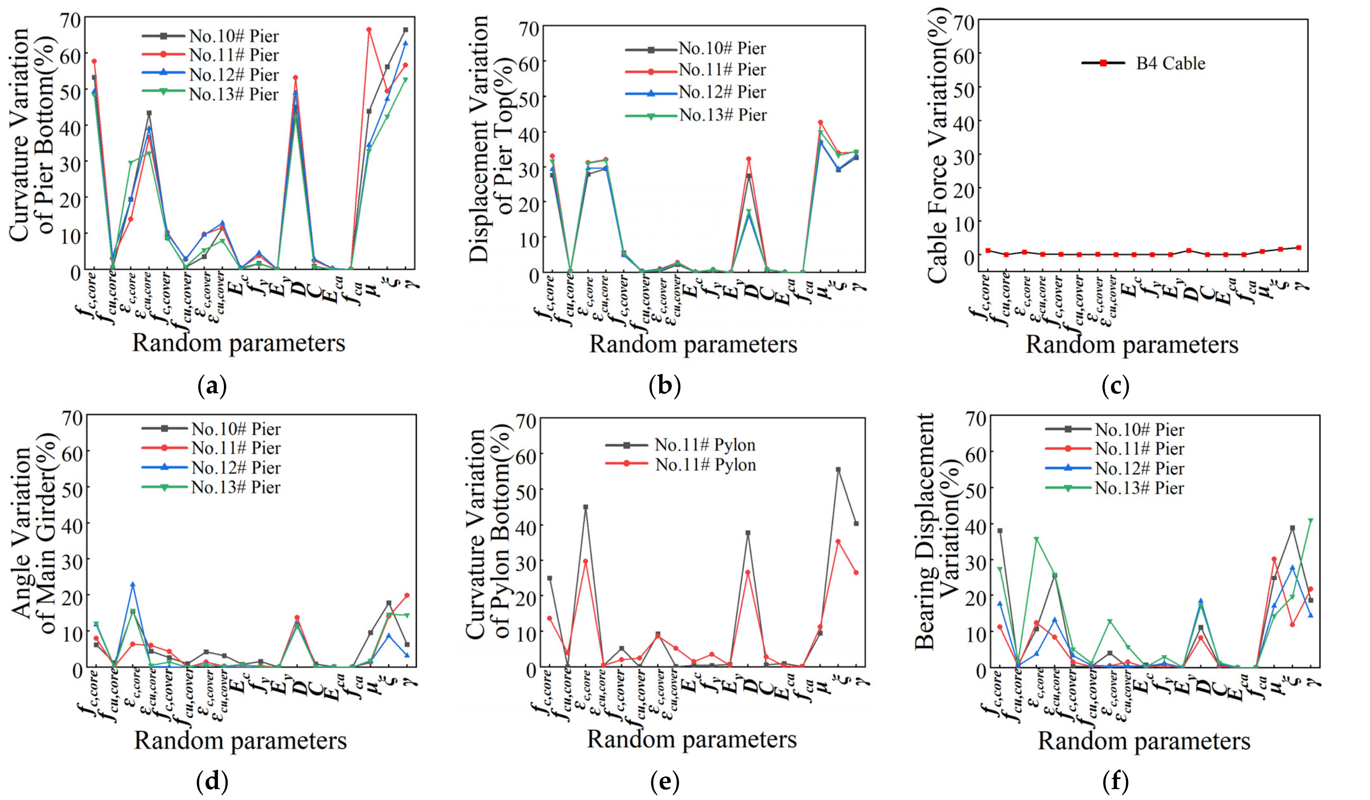

Figure 13. Sensitivity of SFDP under the longitudinal ground motion. (**a**) Curvature sensitivity of pier bottom (**b**) Displacement sensitivity of pier top (**c**) Cable force sensitivity (**d**) Main girder angle sensitivity (**e**) Curvature sensitivity of pylon bottom (**f**) Bearing displacement sensitivity.

According to the nonlinear results calculated by the selected ground motions, the regression analysis of each seismic demand parameter is carried out to obtain its calculated value, and then the influence of ground motion uncertainty is considered.

According to Figure 13a–f, for pier-top displacement under longitudinal ground motions, the maximum influence of bearing friction coefficient is 42%, while the influence of concrete bulk density and damping ratio are nearly the same, at 34.4% and 34.1%, respectively. Meanwhile, the influence of the peak compressive strength of confined concrete, ultimate strain of confined concrete, component size and peak strain of confined concrete are also very close, at 33.2%, 32.2%, 32.3% and 31.3%, respectively. Compared with other random variables, these seven parameters, which are more sensitive, have a great impact on the dynamic response of the pier-top displacement of the extradosed cable-stayed bridge. For main girder angle, the influence of peak strain of confined concrete can reach up to 22.8%, and the maximum impact of concrete bulk density is 19.8%. The influence of damping ratio and component are very close as well, at 17.8% and 17.6%, respectively. Meanwhile, the influence of peak compressive strength of confined concrete is 12.2%, and the friction coefficient of the bearing is 9.6%. The influence of these six parameters is greater than that of the other parameters. For the influence of the pier-bottom curvature, the friction coefficient of bearing can reach 66.4%. The second largest influence on the curvature is concrete bulk density, which can reach 62.7%. The influence of damping ratio is 56.2%, while the peak compressive strength of confined concrete and component size are nearly the same, with influences of 53.3% and 53.2%, respectively. Meanwhile, the influence of the ultimate strain of confined concrete is 43.5%, and that of the ultimate strain of unconfined concrete is 12.8%. In summary, pier-bottom curvature is less sensitive to other parameters, the influences of which are less than 10%. For the curvature of the pylon bottom, the damping ratio has the greatest impact, reaching 55.6%, followed by the peak strain of confined concrete, with an influence of 45.1%. The influence of pylon-section size and height are 43.5%, and that of concrete bulk density is 40.4%. Meanwhile, the impact of the peak compressive strength of confined concrete is 25.1%, and other parameters have little influence on the pylon-bottom curvature. Compared with the other SFDP, there are more parameters that affect the bearing displacement. According to their impact, they are damping ratio, peak compressive strength of confined concrete, concrete bulk density, peak strain of confined concrete, friction coefficient of bearing, component size, ultimate strain of confined concrete and peak strain of unconfined concrete with influences of 53.2%, 45.2%, 41.0%, 35.9%, 30.2%, 29.8%, 26.0% and 12.9%, respectively. Other parameters have little influence on the bearing displacements. The corresponding figures also show that for this type of extradosed cable-stayed bridge, the influence of random parameters on the bearing displacement of each pier and the proportion of variation present different characteristics. In addition, the influences of both the absolute value and sensitivity of random parameters on the cable force are relatively small. The cable force is less sensitive to each parameter, and its variation is relatively small. It further indicates that for this type of bridge, the variation ratio of cable force is less sensitive than other SFDP, and it is difficult to quantify the seismic function damage. The sensitivity Tornado diagram of SFDP affected by random parameters under longitudinal earthquake is shown in Figure 14.

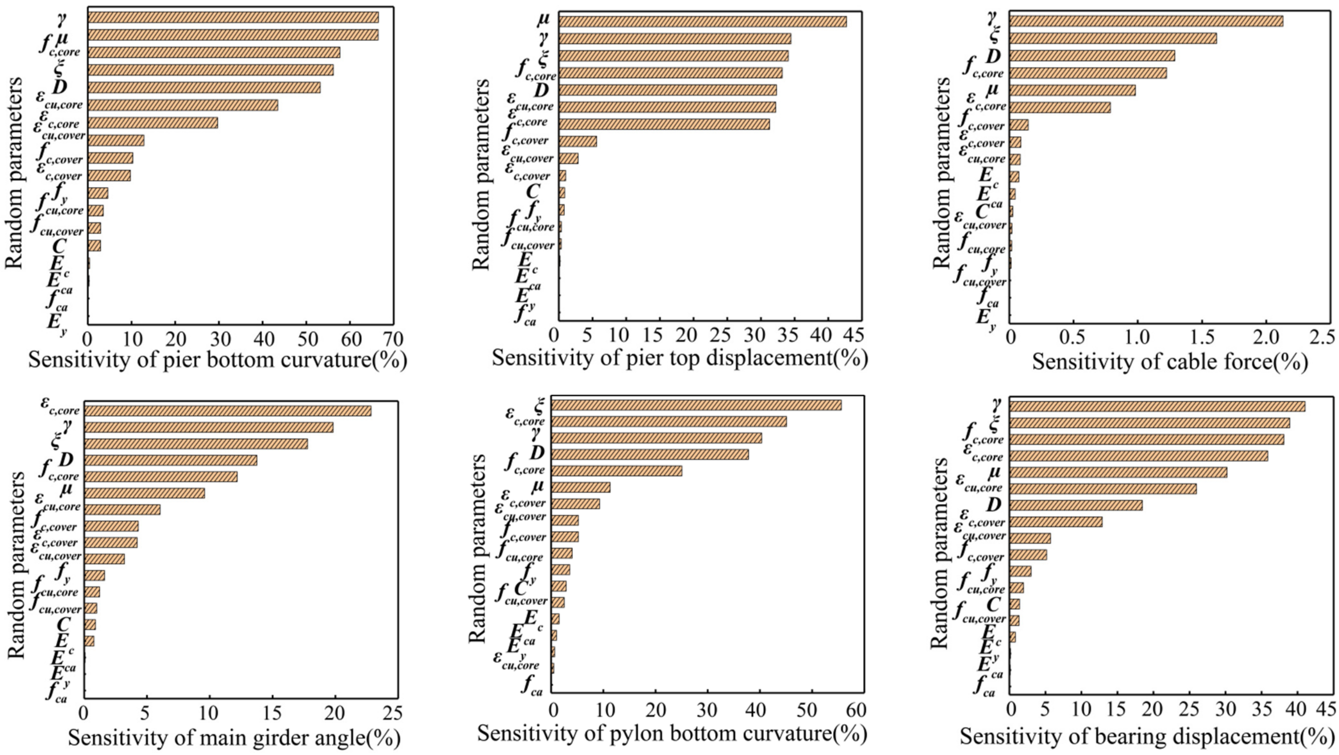

Figure 14. SFDP sensitivity of Tornado Diagram under longitudinal earthquake.

Sensitivity results of SFDP under the transverse ground motion are shown in Figure 15a–f.

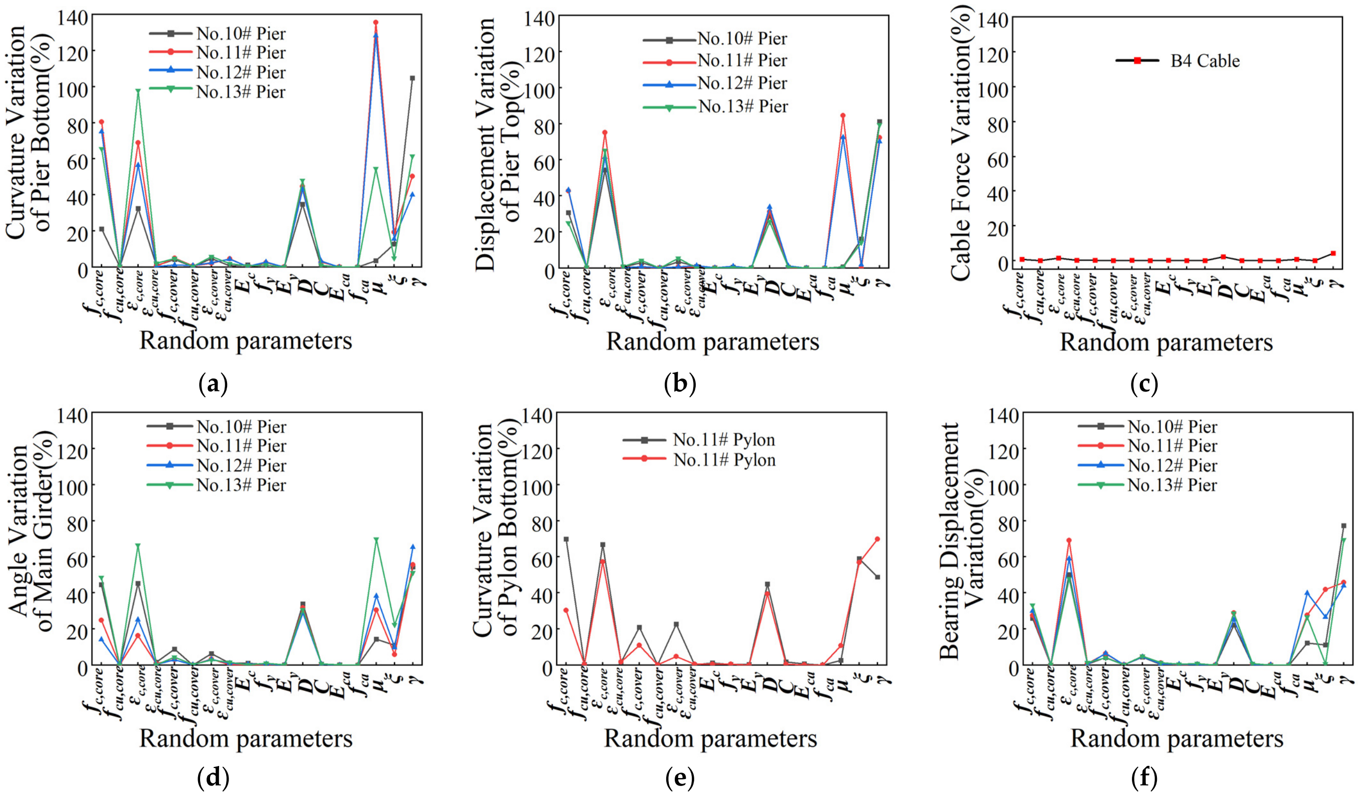

Figure 15. Sensitivity of SFDP under transverse ground motion. (**a**) Curvature sensitivity of pier bottom (**b**) Displacement sensitivity of pier top (**c**) Cable force sensitivity (**d**) Main girder angle sensitivity (**e**) Curvature sensitivity of pylon bottom (**f**) Bearing displacement sensitivity.

According to Figure 15a–f, for pier-top displacement under transverse ground motions, the maximum influence of the bearing friction coefficient is 84.5%, and the influence of concrete bulk density is 81.1%. Meanwhile, the influence of the peak strain of confined concrete, peak compressive strength of confined concrete and component size are 75.2%, 43.2% and 33.8%, respectively. Compared with other random variables, these five parameters, which are more sensitive, have a greater impact on the dynamic response of the pier-top displacement of an extradosed cable-stayed bridge. For the main girder angle, the maximum influence of the bearing friction coefficient is 69.8%, while peak strain of confined concrete and concrete bulk density are very close with the influence of 66.5% and 65.3%, respectively. The influence of the peak compressive strength of confined concrete is 48.6%, and that of component size is 33.8%. The influence of these five parameters is greater than that of other parameters. For the influence of the pier-bottom curvature, the friction coefficient of bearing can reach 135.5%. The second largest influence on the curvature is concrete bulk density, which can reach 104.7%. The influence of the peak strain of confined concrete is 97.8%, and that of peak compressive strength of confined concrete is 80.4%. Meanwhile, the influence of component size is 48.1%. In summary, pier-bottom curvature is less sensitive to other parameters, for which the influences are less than 10%, except for the damping ratio which has an influence of 19.3%. For the curvature of the pylon bottom, the peak compressive strength of confined concrete and concrete bulk density have the greatest impact, which reaches 69.8%, then followed by the peak strain of confined concrete, with an influence of 66.8%. The influence of damping ratio is 59.0%, and that of pylon-section size and height are 44.8%. Meanwhile, the effect of the peak strain of unconfined concrete and peak compressive strength of unconfined concrete are 22.7% and 20.9%, respectively. Furthermore, the influence of other parameters is less than 5%, except for that of the bearing friction coefficient, which has an influence of 10.8%. For the parameters that affect the bearing displacement, according to their impact, they are concrete bulk density, peak strain of confined concrete, damping ratio, friction coefficient of bearing, peak compressive strength of confined concrete and component size with influences of 77.2%, 69.2%, 41.7%, 39.%, 33.1% and 28.9%, respectively. Other parameters have little influence on the bearing displacement, and come to less than 10%. In addition, the influence of cable force is nearly consistent with the that of under longitudinal ground motions, showing the same characteristics with low sensitivity. The sensitivity Tornado diagram of SFDP affected by random parameters under a transverse earthquake is shown in Figure 16.

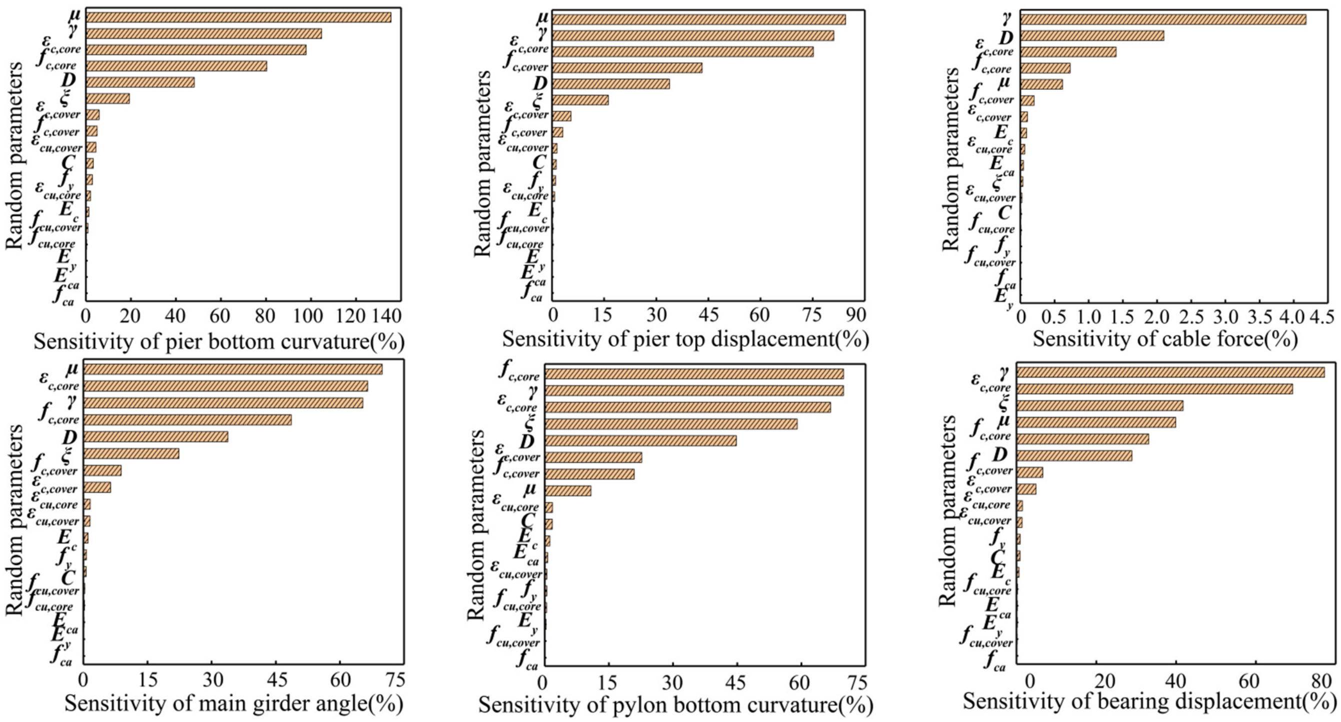

Figure 16. SFDP sensitivity of Tornado Diagram under transverse earthquake.

From Figures 13–16, it can be seen that the cable force has a very low sensitivity to parameter variation. Compared with the influence of random parameters on the SFDP under longitudinal and transverse earthquakes, the friction coefficient of bearing, concrete bulk density, damping ratio, peak compressive strength of confined concrete, component size and peak strain of confined concrete have great influences on the dynamic response of high-speed railway extradosed cable-stayed bridges. These are followed by the parameters of strength and strain of unconfined concrete, the impact of which on the bridge cannot be ignored. The influence of other parameters is slightly insignificant. In other words, the effects of material properties and cross-section should be fully considered for nonlinear dynamic time-history analysis. For example, the fiber section involving the concrete compressive strain and strain should be considered. Therefore, accurate calculation of material parameter characteristics and accurate simulation of structural characteristics are the prerequisites for ensuring accurate and reliable calculation results. For the influence of structural size, the cross-section and pylon height are considered in this paper, for which the error in the bridge dynamic response cannot be ignored. From the point of view of engineering, bridge construction control needs to be strengthened to ensure accuracy of structure size. The research shows that structural uncertainty has a greater impact on the dynamic response of high-speed railway extradosed cable-stayed bridges than that of the traditional static parameter sensitivity analysis. Therefore, it is necessary to clarify the influence of random parameters on the bridge dynamic response, and to explore the relationship between seismic demand and random structural parameters. This is of theoretical and practical significance to clarify the bridge seismic functional damage. Additionally, it is the basis for the subsequent seismic fragility analysis of the bridge.

5. Conclusions

Structural uncertainty is an important factor for seismic fragility analysis of high-speed railway extradosed cable-stayed bridges. It is an effective way to study the influence of random parameters on seismic demand response with nonlinear dynamic time-history analysis by using probabilistic reliability method fully considering the random distribution of the parameters. Based on the above analysis, several conclusions can be drawn as follows:

(1) SFDP are greatly affected by structural uncertainty. The sensitive parameters with the greatest influence on dynamic response are the friction coefficient of bearing, concrete bulk density, damping ratio, peak compressive strength of confined concrete, component size and peak strain of confined concrete. The secondary parameters are the strength and strain of unconfined concrete, the impact of which on the bridge cannot be ignored. The other parameters are insensitive to responses of high-speed railway extradosed cable-stayed bridges;

(2) The effects of material properties and cross-section should be fully considered for nonlinear dynamic time-history analysis. Therefore, accurate calculation of material parameter characteristics and accurate simulation of structural characteristics are the prerequisites for ensuring accurate and reliable calculation results. In addition, the variation ratio of cable force is less sensitive than other SFDP, and it is difficult to quantify the seismic function damage;

(3) Structural uncertainty has a great impact on the dynamic response of high-speed railway extradosed cable-stayed bridges, and it is quite different from traditional static parameter sensitivity analysis. Therefore, it is necessary to clarify the influence of random parameters on the bridge dynamic responses, and to explore the relationship between seismic demand and structural random parameters.

Based on probability and mathematical statistics, this study examined the sensitivity of structural uncertainty of high-speed railway extradosed cable-stayed bridge to seismic fragility demand parameters, and the influence of structural parameter changes on seismic demand parameters was obtained. On the basis of this, a seismic vulnerability analysis of a high-speed railway extradosed cable-stayed bridge will be carried out in the near future. The seismic damage characteristics of the bridge will be systematically studied, and the seismic damage probability of the structure will be proved; this will provide reference for bridge design and post-earthquake operation management. Furthermore, the research on structural health monitoring (SHM) will be carried out in the near future using the method proposed in this paper.

Author Contributions: Conceptualization, M.X.; Software, J.Y. and S.H.; Validation, H.J. and Y.Y.; Investigation, B.S.; Data curation, B.S.; Writing—original draft, J.Y.; Writing—review & editing, M.X.; Funding acquisition, M.X. All authors have read and agreed to the published version of the manuscript.

Funding: This research was funded by the Sichuan Science and Technology Program, grant number 2020YJ0081; the Fundamental Research Funds for the Central Universities, grant number 2682021CX011; and the Science and Technology Research and Development Project of China National Railway Group Co., Ltd., grant number P2019T001. The authors would like to express their sincere gratitude to the sponsor for the financial support.

Institutional Review Board Statement: Not applicable.

Informed Consent Statement: Not applicable.

Data Availability Statement: The data is unavailable due to privacy.

Conflicts of Interest: The authors declare no conflict of interest.

References

1. Lozano-Galant, J.A.; Paya-Zaforteza, I. Analysis of Eduardo Torroja's Tempul Aqueduct an important precursor of modern cable-stayed bridges, extradosed bridges and prestressed concrete. *Eng. Struct.* **2017**, *150*, 955–968. [CrossRef]
2. Meng, X.B.; Zhang, C.H. Extradosed and intradosed cable-stayed bridges with continuous cables: Conceptual consideration. *J. Bridge Eng.* **2014**, *19*, 5–14. [CrossRef]
3. He, X.H.; Wu, T.; Zou, Y.F.; Chen, Y.F.; Guo, H.; Yu, Z.W. Recent developments of high-speed railway bridges in China. *Struct. Infrastruct. Eng.* **2017**, *13*, 1584–1595. [CrossRef]
4. Qin, S.Q.; Gao, Z.Y. Developments and prospects of long-span high-speed railway bridge technologies in China. *Engineering* **2017**, *3*, 787–794. [CrossRef]
5. Yang, S.L.; Pu, Q.H.; Shi, Z.; Hong, Y. Mechanical behavior of steel-concrete composite joints in railway hybrid cable-stayed bridges. *J. Construct. Steel Res.* **2020**, *173*, 106242. [CrossRef]
6. Pu, Q.H.; Yang, S.L.; Shi, Z.; Hong, Y. Fatigue performance of an innovative steel-concrete joint in long-span railway hybrid box girder cable-stayed bridges. *J. Bridge Eng.* **2021**, *26*, 04020129. [CrossRef]
7. Feng, D.M.; Li, A.Q.; Guo, T. Seismic control of a single-tower extradosed railway bridge using the E-Shaped steel damping bearing. *Soil Dyn. Earthq. Eng.* **2020**, *136*, 106249. [CrossRef]
8. Li, S.; Dezfuli, F.H.; Wang, J.Q.; Alam, M.S. Longitudinal seismic response control of long-span cable-stayed bridges using shape memory alloy wire-based lead rubber bearings under near-fault records. *J. Intell. Mater. Syst. Struct.* **2018**, *29*, 703–728. [CrossRef]
9. Zhu, J.; Zhang, W.; Zheng, K.F.; Li, H.G. Seismic design of a long-span cable-stayed bridge with fluid viscous dampers. *Pract. Period. Struct. Des. Constr.* **2016**, *21*, 04015006. [CrossRef]
10. Yang, M.G.; Cai, C.S. Longitudinal vibration control for a suspension bridge subjected to vehicle braking forces and earthquake excitations based on magnetorheological dampers. *J. Vib. Contr.* **2016**, *22*, 3659–3678. [CrossRef]
11. Xu, X.L.; Li, Z.J.; Liu, W.Q.; Feng, D.M.; Li, X.H. Investigation of the wind-resistant performance of seismic viscous dampers on a cable-stayed bridge. *Eng. Struct.* **2017**, *145*, 283–292. [CrossRef]
12. Zhang, X.J.; Zhao, C.Y.; Guo, J. Investigation of seismic performance of super long-span cable-stayed bridges. *Earthq. Struct.* **2018**, *14*, 493–503. [CrossRef]
13. Wei, B.; Hu, Z.L.; He, X.H.; Jiang, L.Z. Evaluation of optimal ground motion intensity measures and seismic fragility analysis of a multi-pylon cable-stayed bridge with super-high piers in Mountainous Areas. *Soil Dyn. Earthq. Eng.* **2020**, *129*, 105945. [CrossRef]
14. Chang, L.; Peng, F.; Ouyang, Y.F.; Elnashai, A.S.; Spencer, B.F. Bridge seismic retrofit program planning to maximize postearthquake transportation network capacity. *J. Infrastruct. Syst.* **2012**, *18*, 75–88. [CrossRef]
15. Gou, H.Y.; Leng, D.; Yang, L.C.; Jia, H.Y. Modeling the cumulative residual deformation of high-speed railway bridge pier subjected to multiple earthquakes. *Earthq. Struct.* **2019**, *17*, 317–327. [CrossRef]
16. Guan, Z.G.; Zhang, J.H.; Li, J.Z. Multilevel performance classifications of tall RC bridge columns toward postearthquake rehabilitation requirements. *J. Bridge Eng.* **2017**, *22*, 04017080. [CrossRef]
17. Zhong, J.; Jeon, J.S.; Yuan, W.C.; DesRoches, R. Impact of spatial variability parameters on seismic fragilities of a cable-stayed bridge subjected to differential support motions. *J. Bridge Eng.* **2017**, *22*, 04017013. [CrossRef]
18. Pang, Y.T.; Wu, X.; Shen, G.Y.; Yuan, W.C. Seismic fragility analysis of cable-stayed bridges considering different sources of uncertainties. *J. Bridge Eng.* **2014**, *19*, 04013015. [CrossRef]
19. Ho, L.V.; Khatir, S.; Roeck, G.D.; Bui-Tien, T.; Wahab, M.A. Finite element model updating of a cable-stayed bridge using metaheuristic algorithms combined with Morris method for sensitivity analysis. *Smart Struct. Syst.* **2020**, *26*, 451–468. [CrossRef]
20. Deco, A.; Bocchini, P.; Frangopol, D.M. A probabilistic approach for the prediction of seismic resilience of bridges. *Earthq. Eng. Struct. Dyn.* **2013**, *42*, 1469–1487. [CrossRef]
21. Wang, P.; Lu, Z.Z.; Tang, Z.C. An application of the Kriging method in global sensitivity analysis with parameter uncertainty. *Appl. Math. Model.* **2013**, *37*, 6543–6555. [CrossRef]
22. Wan, H.P.; Ren, W.X. Parameter selection in finite-element-model updating by global sensitivity analysis using Gaussian process metamodel. *J. Struct. Eng.* **2015**, *141*, 04014164. [CrossRef]
23. Wan, H.P.; Ren, W.X. A residual-based Gaussian process model framework for finite element model updating. *Comput. Struct.* **2015**, *156*, 149–159. [CrossRef]
24. Luedtke, N.; Panzeri, S.; Brown, M.; Broomhead, D.S.; Knowles, J.; Montemurro, M.A.; Kell, D.B. Information-theoretic sensitivity analysis: A general method for credit assignment in complex networks. *J. R. Soc. Interface* **2008**, *5*, 223–235. [CrossRef] [PubMed]
25. Shi, J.X.; Ran, Z.H. Sensitivity analysis of creep effect parameters based on 175 m-span extradosed cable-stayed bridge. In Proceedings of the 4th International Conference on Applied Materials and Manufacturing Technology 2018, Nanchang, China, 25–27 May 2018. [CrossRef]
26. Shi, J.X.; Ran, Z.H. Calculation of creep effect of extradosed cable-stayed bridge based on Midas Civil. In Proceedings of the 4th International Conference on Applied Materials and Manufacturing Technology, Nanchang, China, 25–27 May 2018. [CrossRef]
27. Xie, M.Z.; Yang, Y.Q.; Bu, Y.Z.; Wang, X.W.; Wei, R. Influence of error of unstressed cable length on mechanical behavior of thousand-meter-scale hybrid girder cable-stayed bridge. *J. Highw. Tran. Res. Devel.* **2014**, *8*, 30–36. [CrossRef]
28. Yi, L.X.; Mei, D.P.; Zhou, C. Design of a rail-road asymmetrical low-pylon cable-stayed bridge with a main span of 588 m. *Proc. Inst. Civ. Eng. Bridge Eng.* **2020**, *173*, 190–197. [CrossRef]

29. Nariman, N.A. Aerodynamic stability parameters optimization and global sensitivity analysis for a cable stayed bridge. *KSCE J. Civil Eng.* **2017**, *21*, 1866–1881. [CrossRef]
30. Wu, F.W.; Xu, C.; Zhao, L. Analysis on sensitivity of stochastic seismic response parameters of super-long-span cable-stayed bridges. *Tiedao Xuebao J. China Railw. Soc.* **2014**, *36*, 107–114. [CrossRef]
31. Jia, H.Y.; Zhang, D.Y.; Zheng, S.X.; Xie, W.C.; Pandey, M.D. Local site effects on a high-pier railway bridge under tridirectional spatial excitations: Nonstationary stochastic analysis. *Soil Dyn. Earthq. Eng.* **2013**, *52*, 55–69. [CrossRef]
32. Jia, H.Y.; Lan, X.L.; Zheng, S.X.; Li, L.P.; Liu, C.Q. Assessment on required separation length between adjacent bridge segments to avoid pounding. *Soil Dyn. Earthq. Eng.* **2019**, *120*, 398–407. [CrossRef]
33. Jia, H.Y.; Yue, W.Q.; Zheng, S.X.; Gou, H.Y.; Zhao, C.H.; You, G. Time-dependent pounding probability analysis between adjacent decks of bridges under non-stationary stochastic seismic excitations. *Structure* **2020**, *28*, 2355–2366. [CrossRef]
34. Jahangiri, V.; Yazdani, M. Seismic reliability and limit state risk evaluation of plain concrete arch bridge. *Struct. Infrastruct. Eng.* **2021**, *17*, 170–190. [CrossRef]
35. Homaei, F.; Yazdani, M. The probabilistic seismic assessment of aged concrete arch bridges: The role of soil-structure interaction. *Structures* **2020**, *28*, 894–904. [CrossRef]
36. Helton, J.C.; Davis, F.J. Latin hypercube sampling and the propagation of uncertainty in analyses of complex systems. *Reliability Eng. Syst. Saf.* **2003**, *81*, 23–69. [CrossRef]
37. Olsson, A.; Sandberg, G.; Dahlblom, O. On Latin hypercube sampling for structural reliability analysis. *Struct. Saf.* **2003**, *25*, 47–68. [CrossRef]
38. Au, S.K.; Beck, J.L. A new adaptive importance sampling scheme for reliability calculations. *Struct. Saf.* **1999**, *21*, 135–158. [CrossRef]
39. Liu, P.L.; Der, K.A. Multivariate distribution models with prescribed marginals and covariances. *Probab. Eng. Mech.* **1986**, *1*, 105–112. [CrossRef]
40. Yuan, B.; Chen, M.; Chen, W.; Luo, Q.; Li, H. Effect of Pile-Soil Relative Stiffness on Deformation Characteristics of the Laterally Loaded Pile. *Adv. Mater. Sci. Eng.* **2022**, *2022*, 4913887. [CrossRef]
41. Barbato, M.; Gu, Q.; Conte, J.P. Probabilistic Push-Over analysis of structural and soil-structure systems. *J. Struct. Eng.* **2010**, *136*, 1330–1341. [CrossRef]
42. Thomos, G.C.; Trezos, C.G. Examination of the probabilistic response of reinforced concrete structures under static non-linear analysis. *Eng. Struct.* **2006**, *28*, 120–133. [CrossRef]
43. Porter, K.A.; Beck, J.L.; Shaikhutdinov, R.V. Sensitivity of building loss estimates to major uncertain variables. *Earthq. Spectra* **2002**, *18*, 719–743. [CrossRef]